CHEMISTRY OF MATERIALS

Article

pubs.acs.org/cm

Electron Acceptors Based on α-Substituted Perylene Diimide (PDI) for Organic Solar Cells

Donglin Zhao,[†,▽] Qinghe Wu,[†,▽] Zhengxu Cai,[†] Tianyue Zheng,[†] Wei Chen,[‡,§] Jessica Lu,[†] and Luping Yu*[,†]

[†]Department of Chemistry and The James Franck Institute, The University of Chicago, 929 East 57th Street, Chicago, Illinois 60637, United States

[‡]Materials Science Division, Argonne National Laboratory, 9700 Cass Avenue, Lemont, Illinois 60439, United States

[§]Institute for Molecular Engineering, The University of Chicago, 5747 South Ellis Avenue, Chicago, Illinois 60637, United States

Supporting Information

ABSTRACT: Perylene diimide (PDI) derivatives functionalized at the ortho-position (αPPID, αPBDT) were synthesized and used as electron acceptors in non-fullerene organic photovoltaic cells. Because of the good planarity and strong π-stacking of ortho-functionalized PDI, the αPPID and αPBDT exhibit a strong tendency to form aggregates, which endow the materials with high electron mobility. The inverted OPVs employing αPDI-based compounds as the acceptors and PBT7-Th as the donor give the highest power conversion efficiency (PCE) values: 4.92% for αPBDT-based devices and 3.61% for αPPID-based devices, which are, respectively, 39% and 4% higher than that of their β-substituted counterparts βPBDT and βPPID. Charge separation studies show more efficient exciton dissociation at interfaces between αPDI-based compounds and PTB7-Th. The results suggest that α-substituted PDI derivatives are more promising electron acceptors for organic photovoltaic (OPV) components than β-isomers.

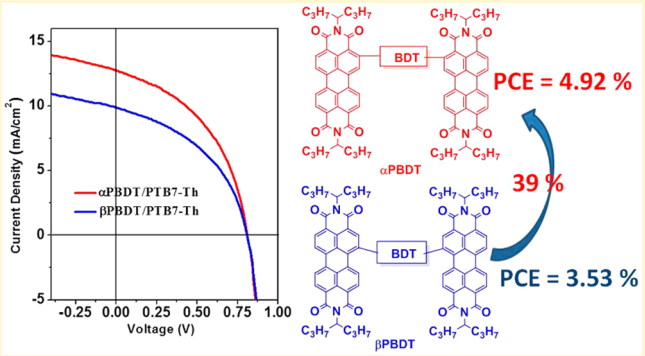

INTRODUCTION

Organic photovoltaic (OPV) solar cells have advanced tremendously over the past several years. However, two challenges remain in the field. One is to further increase the power conversion efficiency (PCE). Currently, PCE values as high as >11% have been reported in small devices.[1,2] This value is encouraging, but not enough for significant commercial exploration. Fortunately, the pace of progress suggests that this problem is solvable. The significant achievement in high PCE values has been made possible in bulk heterojunction (BHJ) solar cells which utilize the conjugated molecules or polymers as the donor and fullerene derivatives as the acceptor.[3−6] The second challenge is the cost of materials. Both donor and acceptor OPV materials are rather expensive. Because of the variety of different donor polymers available, the cost for donor materials can be managed. Although the fullerene derivatives ($PC_{61}BM$, $PC_{71}BM$) have superior electron-accepting properties, their drawbacks are also clear: high cost, limited visible light absorption, and instability of morphology in blend film, all of which have hindered their industrial application and further improvements in device performance.[7]

Recently, intensive research interest has been devoted to exploring new electron acceptors via electron-deficient subunits (such as diketopyrrolopyrrole, dicyanovinyl, naphthalene diimide (NDI), and perylene diimide (PDI)) to replace the PCBM.[8−14] Among them, PDI is the most promising motif for use in electron-deficient acceptors for OPV applications.[11,15−18] PDI exhibits several appealing properties, including low cost, chemical robustness, ease of functionalization, suitable optical absorption range, and strong electron deficiency.[15,19,20] Because of the strong tendency toward aggregation of the extended conjugated backbone in PDI, two strategies were adopted to reduce the strong π-stacking, in order to enhance the processability of materials and form favorable BHJ domains. One is to disrupt the strong π−π interaction of PDI by introducing torsion in the conjugated backbone, such as twisted PDI dimers connected at the N-position or bay positions (1-, 6-, 7-, and 12-positions).[21−26] Another is to synthesize A-D-A (Acceptor−Donor−Acceptor) molecules with the donor coupled to PDIs at the bay positions.[15,17,27] Both approaches have been effective in generating non-fullerene electron acceptors that show improved OPV performance, compared to single PDI molecules.[15,18] Unfortunately, the functionalization at the bay positions of PDI leads to twisting of the perylene core, which disrupts the π-stacking of π-surface and diminishes the electron transport in the bulk state in the thin-film

Received: November 25, 2015
Revised: January 20, 2016
Published: January 20, 2016

DOI: 10.1021/acs.chemmater.5b04570
Chem. Mater. 2016, 28, 1139−1146

Scheme 1. Synthetic Procedure of PDI-2Bpin (Top) and the Synthesis of αPPID, βPPID, αPBDT, and βPBDT (Bottom)

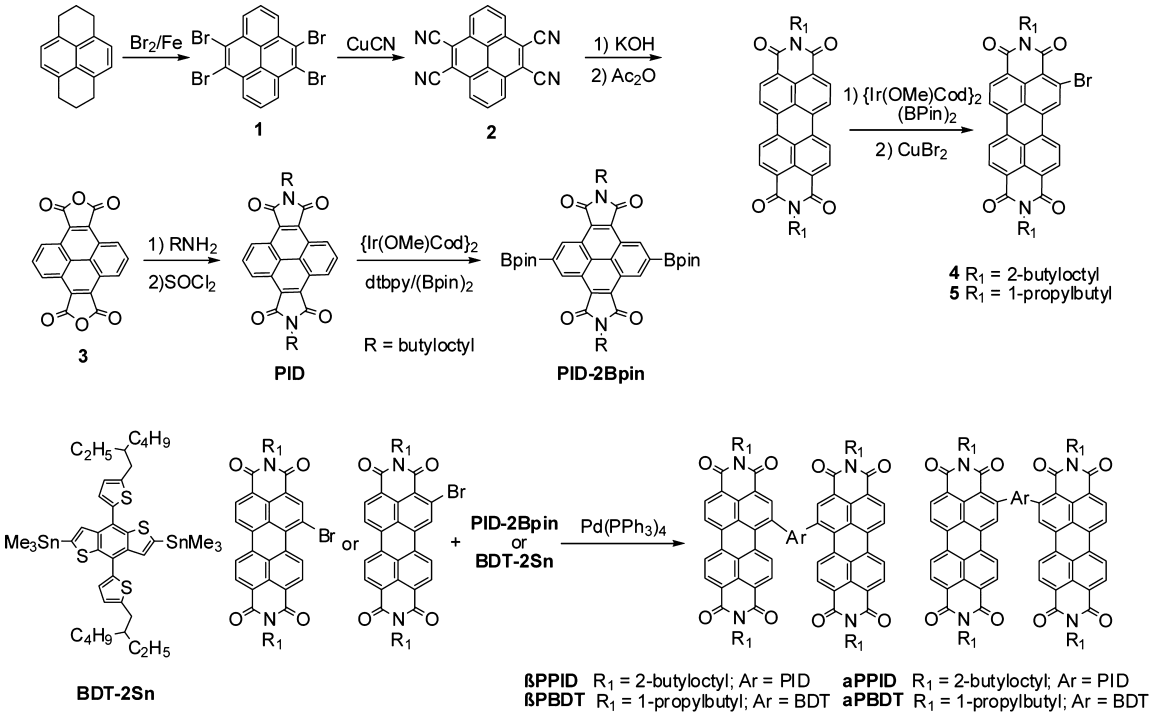

transistors.[28−31] High electron mobility is also highly desired to achieve high OPV performance in the solar cells. Therefore, strategies to functionalize PDI without introducing torsion in the perylene core are desirable. In this paper, we describe the design and synthesis of α-monobrominated PDI and developed A-D-A and A-wA-A acceptors by coupling donor (D)/weak acceptor (wA) with α-bromo PDI. Detailed studies indicate that α-substituted PDI derivatives with A-D-A structure are indeed promising electron acceptors.

RESULT AND DISCUSSION

Design and Synthesis of Compounds. The selective functionalization of the ortho-position (2-, 5-, 8-, and 11-positions) of PDI by introducing boron, alkyl, and aryl substituent are known,[32−35] by which the optical, electrical, packing, and film-forming properties of PDI derivatives can be tuned. Evidence exists that the perturbation of the planarity of the perylene core due to functionalization at ortho-position of PDI is minimized.[36,37] Furthermore, functional groups in the ortho-position exert limited steric hindrance with PDI. Structural analysis on single crystals of NDI-4TH show that, because of the strong interaction between oxygen (C═O in NDI) and proton (C−H in adjacent thiophene),[38] the dihedral angle between the thiophene ring and NDI core is only 25°, which is much smaller than the simulated dihedral angle (55°−60°) between adjacent thiophene ring and PDI when thiophene attached at the bay position of PDI.[39] Considering the similarity between the ortho-positions of NDI and PDI, it is safe to assume that connecting aromatic units such as thiophenyl groups at the ortho-position of PDI can significantly increase the coplanarity of the desired compounds, which will benefit the transport of electrons. Based on these considerations, we synthesized α-monobrominated PDI as a new building block to develop electron acceptors. In our previous work, we demonstrated that polarity in acceptor polymers is also important for achieving high solar cell efficiency.[40] To compare the effect of polarity, we developed A-D-A and A-wA-A acceptors. BDT is used as the donor. Pyrene diimide (PID) was synthesized and used as the weak acceptor unit. This novel five-ring diimide allows functionalization at the 2- and 7-positions that are much less sterically hindered than similar positions in other diimides, such as PDI and NDI.[41]

The α-monobrominated PDI (compounds **4** and **5**) was synthesized in a two-step, one-pot reaction. (A schematic depiction of the synthesis procedures for PDI-2Bpin, as well as αPPID, βPPID, αPBDT, and βPBDT, is shown in Scheme 1.) The α-position of PDI was first functionalized with pinacolatoboron (Bpin) group in a modified Ir-catalyzed reaction, developed by the Shinokubo and Osuka group.[34] The reaction mixture was treated with $CuBr_2$ without separation. The synthesis of the weaker acceptor PID-2Bpin starts from commercially available material 1,2,3,6,7,8-hexahydropyrene, which was brominated with bromine for 30 min, yielding 4,5,9,10-tetrabromo-1,2,3,6,7,8-hexahydropyrene. The use of an excessive amount of bromine in the reaction medium can convert 4,5,9,10-tetrabromo-1,2,3,6,7,8-hexahydropyrene to 4,5,9,10-tetrabromopyrene (compound **1**) under light. Compound **1** was then cyanated to compound **2**, which is further hydrolyzed to form compound **3**. Because compounds **1**, **2**, and **3** exhibit poor solubility in common solvents, the crude products were used directly without further purification. Imidization with alkylamine led to the formation of PID. It was found that the reaction of PID with bromine in a $CHCl_3$/CF_3COOH/H_2SO_4 leads to undesired bromination at the 1-, 3-, 6-, and 8-positions. Selective functionalization of the 2- and 7-positions of PID with Bpin was realized by a sterically controlled Ir-catalyzed reaction.[42] The target compounds—αPPID, βPPID, αPBDT, and βPBDT—were synthesized via palladium-mediated Stille or Suzuki coupling reactions. These compounds exhibit high solubility in common solvents such as chloroform and chlorobenzene. Their structures were charac-

DOI: 10.1021/acs.chemmater.5b04570
Chem. Mater. 2016, 28, 1139−1146

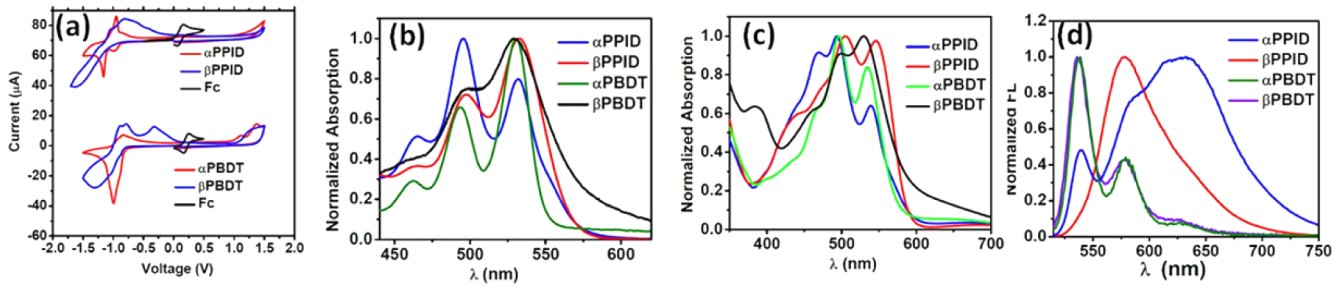

Figure 1. (a) Cyclic voltammograms of the films, absorption ((b) solution absorption and (c) film absorption), and (d) solution emission spectra of *α*PPID, *β*PPID, *α*PBDT, and *β*PBDT.

Table 1. Electrochemical and Optical Data and DFT Calculation Results of *α*PPID, *β*PPID, *α*PBDT, and *β*PBDT

	Observed		Calculated						
	LUMO (eV)	HOMO (eV)	LUMO^{Cal} (eV)	HOMO^{Cal} (eV)	dihedral angle (deg)	bay angle (deg)	I^{00}/I^{01} sol	I^{00}/I^{01} film	quantum yield, QY (%)
*α*PPID	−3.84	−5.86[a]	−4.19	−5.66	51.4	2.0	0.80	0.77	14
*β*PPID	−3.79	−5.87[a]	−4.21	−5.59	48.8	20.2	1.38	0.98	43
*α*PBDT	−3.78	−5.60	−4.13	−4.80	45.96	4.5	1.52	0.88	0.25
*β*PBDT	−3.76	−5.64	−4.13	−5.05	46.79	18.9	1.33	1.11	0.01

[a]The HOMO energy level was calculated using the following equation: $E_{HOMO} = E_{LUMO} - E_g^{opt}$.

terized and confirmed via various spectroscopic techniques, which are shown in the Supporting Information.

Electronic and Optical Properties. Lowest unoccupied molecular orbital (LUMO) energy levels for different imide building motif were determined by cyclic voltammetry (CV) to be −3.16 eV for PID, −3.57 eV for NDI, and −3.83 eV for PDI, which is a trend that is in agreement with that obtained from theoretical calculation (see Figure S1 in the Supporting Information).[43] This high LUMO suggests that PID is a weak acceptor subunit and that the electron-withdrawing ability of the five-member diimide is weaker than that of six-member diimide.[44] CV was also employed to investigate the electrochemical properties of the four PDI-based compounds (Figure 1a). LUMO and highest occupied molecular orbital (HOMO) energy values of the four compounds (*α*PPID, *β*PPID, *α*PBDT, and *β*PBDT) are listed in Table 1. The four compounds show almost-identical LUMO energy levels, while the HOMO energy levels of compounds containing PID are slightly lower than those of the compounds containing BDT, because of the electron-withdrawing nature of PID and electron-donating nature of BDT. The energy levels of the four compounds all match well with that of PTB7-Th, with enough energy offset for both electron and hole transfer to each other to be favorable.[45]

UV-vis absorption spectra of the four compounds were recorded both in solution and in the solid film (see Figures 1b and 1c). They all exhibit three vibronic peaks, resembling PDI monomer.[33,34] The *β*-isomers showed red-shifted band edges, likely due to more extended electron delocalization. However, the absorption peaks for *α*PPID at 495 nm in solution are stronger than other three compounds and resemble its film absorption, which suggest a strong tendency of *α*PPID to form aggregates in the dilute solution. In the film absorption spectra, both *α*-substituted compounds exhibit a stronger 0−1 (I^{01}) absorption peak than the 0−0 (I^{00}) transition, while *β*-substituted compounds show similar or weaker intensity for 0−1 in solid state than the 0−0 transition. The decrease in the ratio of 0−0 to 0−1 transition intensity from solution to solid state for four compounds (blue-shift in absorption maxima) indicates the formation of H-aggregates. This decrease is largest for *α*PBDT, which implies strong intermolecular *π*−*π* interaction and high packing order of *α*PBDT, which is beneficial for charge transport[28,46−48]. The solution-phase emission spectra for the four compounds are shown in Figure 1d, and the quantum yield (QY) for the emission is shown in Table 1. The *α*PBDT and *β*PBDT have similar, but weak emission spectra (low QY), whose shape resembles that of the PDI monomer. This may indicate quenching caused by intramolecular charge transfer. The *α*PPID and *β*PPID show a large red-shift emission peak. The *α*PPID also shows a concentration-dependent emission spectrum (see Figure S5 in the Supporting Information), indicating the formation of excimers, as evidenced by the broad peak at 600−700 nm that coincide with reported PDI excimer.[48−51] The results indicate that the *π*-system in *α*PPID is closely packed, because of its good planarity. The excimer emission in *α*PPID is overlapped with the weak emission from monomeric *α*PPID. The emission spectrum of *β*PPID only has one peak at 579 nm which corresponds to the 1−0 transition of PDI, which may be due to special electronic features of the twisted PDI core.

DFT Calculation. In order to gain more insight into the structural and electronic difference between *α*-substituted and *β*-substituted PDIs, density functional theory (DFT) calculations by using the Gaussian package D3BJTPSS/def2-TZVP were carried out to evaluate the frontier molecular orbitals and structures of the four compounds.[52] To facilitate the calculation, the long alkyl chains were replaced with a methyl group. A pictorial presentation of the LUMO and HOMO orbitals of the four compounds is shown as Figure S2 in the Supporting Information, and the energy levels and torsional angles are summarized in Table 1. The torsion angle of the PDI backbone at the bay area is 2.0° for *α*PPDI and 4.5° for *α*PBDT, which is much smaller than 20.2° for *β*PPDI and 18.9° for *β*PBDT. The dihedral angle between the linker and PDI for *α*-PDI derivatives is similar to that for *β*-isomers, according to the calculation. Thus, the good planarity of *α*-position functionalized PDI could facilitate close packing and enhance electron transport.

DOI: 10.1021/acs.chemmater.5b04570
Chem. Mater. 2016, 28, 1139−1146

Table 2. Parameters Summary of Solar Cell Devices with αPPID, βPPID, αPBDT, and βPBDT as Acceptors and PTB7-Th as a Donor

acceptor	J_{sc} (mA cm^{-2})	V_{oc} (V)	FF	Eff (%) (best device)	μ_e (cm^2 V^{-1} s^{-1})	μ_h (cm^2 V^{-1} s^{-1})	RMS (nm)
αPPID	10.15 ± 0.5	0.77 ± 0.01	0.44 ± 0.01	3.49 ± 0.12 (3.61)	4.46×10^{-4}	3.12×10^{-5}	0.7
βPPID	9.14 ± 0.4	0.78 ± 0.01	0.45 ± 0.01	3.20 ± 0.27 (3.47)	3.48×10^{-4}	5.33×10^{-5}	0.7
αPBDT	12.74 ± 0.4	0.81 ± 0.01	0.46 ± 0.01	4.76 ± 0.16 (4.92)	8.00×10^{-4}	1.79×10^{-5}	1
βPBDT	9.80 ± 0.3	0.81 ± 0.01	0.44 ± 0.01	3.49 ± 0.04 (3.53)	4.81×10^{-4}	1.04×10^{-5}	0.9

OPV Properties and Active Layer Characterization. From the CV studies, the energy levels of these compounds as acceptors match those of PTB7-Th as a donor. We prepared the inverted solar cells with a configuration of ITO/ZnO/active layer/MoO_3/Al to evaluate the photovoltaic properties of these small molecules. A donor/acceptor ratio of 1:1.5 was spin-cast from hot chlorobenzene with 5% 1-chloronaphthalene as an additive and an active layer with a thickness of ∼100 nm was formed. The above conditions needed to make an active layer gives the best OPV performance for all four PDI-based molecules. The $J-V$ characteristics of these OPV cells are shown in Table 2, and $J-V$ curves are plotted in Figure 2a. The

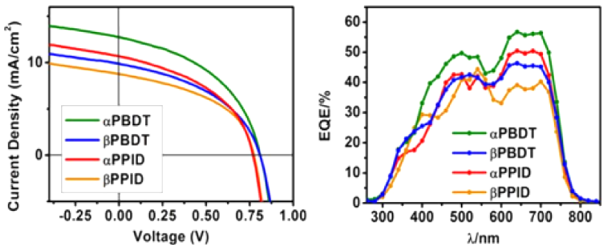

Figure 2. (a) $J-V$ characteristics and (b) external quantum efficiency (EQE) spectra of solar cell devices using αPPID (red), βPPID (orange), αPBDT (green), and βPBDT (blue) as acceptors and PTB7-Th as the donor.

device results demonstrate that αPDI-based acceptors show very similar open-circuit voltage (V_{oc}) values as that of βPDI-based acceptors. This is anticipated because of the similarity between their LUMO energy levels, which are close, because they have the same linker.[53] For the BDT-linked acceptors, an average PCE of 4.76% for αPBDT is achieved with a short-circuit current density (J_{sc}) of 12.74 mA/cm^2, V_{oc} = 0.81 V, and a fill factor (FF) of 0.46, which is 36% higher than that for βPBDT. The PCE enhancement is largely due to much higher J_{sc} values for αPBDT (12.74 mA/cm^2) than that for βPBDT (9.80 mA/cm^2). The slightly higher PCE of 3.49% for αPPID than that for βPPID (3.20%) can be attributed to a better intermolecular packing in αPPID than in βPPID. This is consistent with the smaller twisted angle in the αPDI moiety in DFT calculation and the excimer formation in αPPID solution shown by the emission spectrum, which led to a better J_{sc} value of 10.15 mA/cm^2 than that for βPPID (9.14 mA/cm^2). These results indicated that acceptors based on αPDI exhibit superior photovoltaic performance over that of βPDI-based acceptors. The bottleneck for these devices is the low FF value of 0.45 ± 0.01, which is far below the values for polymer/fullerene devices (>0.6).[6,24,54] Further device optimization is underway to explore the potential of αPDI-based acceptors.

The external quantum efficiency (EQE) of the optimal αPPID/βPPID/αPBDT/βPBDT:PTB7-Th devices were measured and are shown in Figure 2b. The J_{sc} values calculated from the EQE all have <10% deviation from J_{sc} measured in solar cell devices. The results shed some light on the PCE performance of these OPV cells. It can be seen that all four devices show broad EQE spectra from 300 nm to 800 nm. The photon absorption for donor polymer PTB7-Th is between 550 nm and 800 nm. In this region, the quantum efficiency for PTB7-Th blended with α-isomers is higher than PTB7-Th blends with related β-isomers, indicating more efficient charge separation with α-isomers. The quantum efficiency for αPBDT is obviously higher than all others in the entire spectrum.

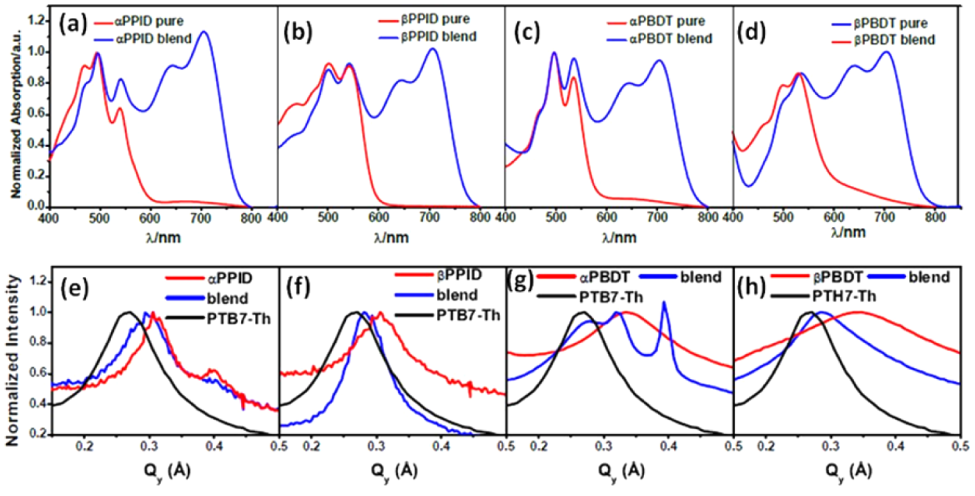

Figure 3. Absorption spectrum of (a) neat αPPID and αPPID/PTB7-Th blend film, (b) neat βPPID and βPPID/PTB7-Th blend film, (c) neat αPBDT and αPBDT/PTB7-Th blend film, and (d) neat βPBDT and βPBDT/PTB7-Th blend film. Also shown are the in-plane 2D GIWAXS patterns of (e) neat PTB7-Th, αPPID, and their blend film; (f) neat PTB7-Th, βPPID, and their blend film; (g) neat PTB7-Th, αPBDT, and their blend film; and (h) neat PTB7-Th, βPBDT, and their blend film.

DOI: 10.1021/acs.chemmater.5b04570
Chem. Mater. 2016, 28, 1139−1146

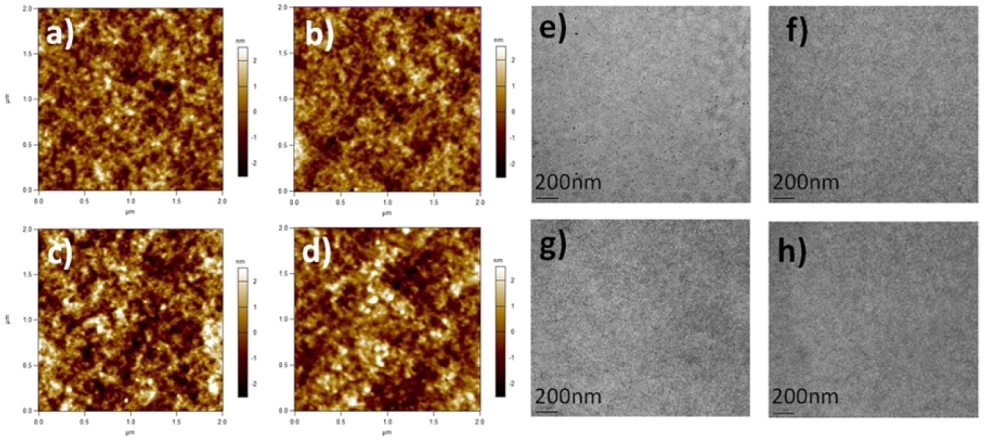

Figure 4. Atomic force microscopy (AFM) of films of (a) αPPID/PTB7-Th, (b) βPPID/PTB7-Th, (c) αPBDT/PTB7-Th, and (d) βPBDT/PTB7-Th. Also shown are transmission electron microscopy (TEM) images of the films of (e) αPPID/PTB7-Th, (f) βPPID/PTB7-Th, (g) αPBDT/PTB7-Th, and (h) βPBDT/PTB7-Th.

The absorption spectrum of the active layer blends were further measured and recorded in Figures 3a–d. It was found that the absorption spectrum of αPBDT in the blend film is very similar to that in pure film. The αPBDT not only maintains the two sharp and distinctive perylene diimide 0–0 and 0–1 vibrational peaks at 540 and 495 nm, but it also has a shoulder of 0–2 transition at 450 nm. However, in βPPID and βPBDT's blend films, 0–0 and 0–1 transitions are broadened and almost merged with each other, while intensity of the 0–2 transition for αPPID blend film is significantly decreased, which is different from their pure film absorption spectrum. A possible explanation for this phenomenon is that the αPBDT blend films maintain the same packing order as in the pure αPBDT domains.

The grazing-incidence wide-angle X-ray scattering (GIWAXS) measurement was employed to investigate the crystallinity of the neat and blend films (see Figure S8 in the Supporting Information). The in-plane GIWAXS patterns of the neat PTB7-Th, αPPID, βPPID, αPBDT, and βPBDT films and the corresponding blend films are shown in Figures 3e–h. The neat films of PTB7-Th, αPPID, βPPID, αPBDT, and βPBDT show Bragg reflections at $q_y \approx 0.27$, 0.31, 0.305, 0.34, and 0.34 Å^{-1}, corresponding to *d*-spacings of 23.3, 20.3, 20.6, 18.5, and 18.5 Å, respectively. This peak can be assigned to lateral spacing along the side chains. The βPPID/PTB7-Th and βPBDT/PTB7-Th blend films both exhibit Bragg reflections at $q_y \approx 0.28$ Å^{-1} (22.4 Å) that are very close to 0.27 Å^{-1} for the neat donor polymer PTB7-Th. Three diffraction peaks at 0.275 Å^{-1} (22.8 Å), 0.33 Å^{-1} (19.0 Å), and 0.40 Å^{-1} (15.7 Å) was observed for αPBDT/PTB7-Th blend film. The peaks at 0.275 Å^{-1} and 0.33 Å^{-1} are from the diffraction of PTB7-Th and αPBDT, respectively, which implies both pure donor and acceptor domains exist in the blend film. This result is in good agreement with the observation in the absorption spectrum of αPBDT/PTB7-Th blend film. The αPPID/PTB7-Th blend film demonstrates two diffraction peaks, at 0.305 Å^{-1} (18.0 Å) and 0.40 Å^{-1} (15.7 Å). The peaks at 0.305 Å^{-1} are most likely from the diffraction of αPPID. However, it is surprising to observe the enhanced sharp peak at $q_y = 0.40$ Å^{-1}. It seems that the polymer/acceptor interaction directed αPBDT to self-assemble in more-ordered structures, which may be the reason for the observed high electron mobility. The blend film absorption and GIWAXS data both confirm that α-isomers of these acceptors (αPPID, αPBDT) maintain the pure domains and the same packing order in the blend films, which may be due to their strong intermolecular interaction resulting from good planarity of the α-substituted PDI derivative.

The electron and hole mobility of these four devices also help to understand the structure/property relationship. These were measured by the space-charge-limited current method with the device structure of ITO/ZnO/PDIs:PTB7-Th/Ca/Al for e^- and ITO/PEDOT:PSS/PDIs:PTB7-Th/MoO_3/Al for h^+. The electron mobility was calculated to be 4.46×10^{-4}, 3.48×10^{-4}, 8.00×10^{-4}, and 4.81×10^{-4} cm^2 V^{-1} s^{-1} for the αPPID-, βPPID-, αPBDT-, and βPBDT-based devices, while the hole mobility is 3.12×10^{-5}, 5.33×10^{-5}, 1.79×10^{-5}, and 1.04×10^{-5} cm^2 V^{-1} s^{-1}, respectively. (Summarized in Table 2.) It is clear that the αPDI-based compounds exhibited relatively higher electron mobility than their βPDI-based counterparts, which is likely the consequence of better planarity of the α-substituted PDI moieties and stronger intermolecular interaction of αPPID and αPBDT, as shown in the film absorption spectrum. The electron mobility of the hole is roughly 1 order of magnitude lower than the corresponding electron mobility for the four devices. The unbalanced hole and electron mobility partially account for the relatively low OPV device performance.

The active blend films of these devices exhibit similar morphologies, as characterized by atomic force microscopy (AFM) and transmission electron microscopy (TEM) (see Figure 4). AFM height images in Figure 4 (with dimensions of 2 μm × 2 μm) show that the device blends have similar features and comparatively similar smoothness. The root-mean-square (RMS) roughness values of the αPPID and βPPID blend films are 0.7 and 0.7 nm. While the surface for blend films of BDT-linked compounds are rougher, with RMS values of 0.9 and 1 nm for αPBDT and βPBDT, respectively (see Table 2). The TEM images of the four blends are also similar; this is probably due to the weak contrast between the donor polymer and the non-fullerene acceptor. The AFM and TEM studies suggest that the solar cell efficiency difference between the four compounds is not due to blend morphology.

Charge Separation and Recombination Dynamics. To better understand the OPV performance, the exciton dissociation, and carrier collection process, the charge dissociation probability $P(E,T)$ was investigated according to

DOI: 10.1021/acs.chemmater.5b04570
Chem. Mater. 2016, 28, 1139–1146

the reported method.[15,55,56] As shown in Figure 5a, the photo current density J_{ph} (defined by $J_L - J_D$, where J_L and J_D are the

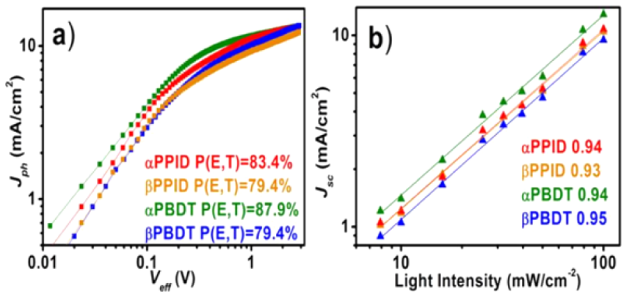

Figure 5. (a) Photocurrent density (J_{ph}) versus effective voltage (V_{eff}) characteristics of the four devices; (b) short current density (J_{sc}) versus the light density of the four devices.

light and dark current densities, respectively) is plotted against the effective voltage V_{eff} (defined by $V_0 - V$, where V_0 is the voltage at $J_{ph} = 0$) on a logarithmic scale. We assume that J_{ph} reaches its saturation (J_{sat}) at high reverse voltage, which means that all the photogenerated exitons are dissociated to free charge carriers and collected by the electrodes. $P(E,T)$ is defined as

$$P(E, T) = \frac{J_{ph}}{J_{sat}}$$

The calculated $P(E,T)$ values under J_{sc} conditions for βPPID and βPBDT are both 79%, while the αPPID and αPBDT devices have higher dissociation probabilities (83% and 88%, respectively). The higher $P(E,T)$ values of αPPID and αPBDT indicate more efficient exciton dissociation at interfaces between αPDI-based compounds and PTB7-Th, which is in good agreement with the higher J_{sc} values of αPPID- and αPBDT-based devices. In order to gain more insight into recombination kinetics, the measurement of J_{sc}, as a function of illumination intensity, was carried out according to the literature.[57,58] In Figure 5b, the linear scaling of photocurrent to light intensity was observed for all four devices and the exponential factors for αP-PID:PTB7-Th, βPPID:PTB7-Th, αPBDT:PTB7-Th, and βPBDT:PTB7-Th devices are 0.95, 0.94, 0.93, and 0.95, respectively. The high and similar values mean that the bimolecular recombination in all four devices is comparatively weak, which is consistent with their similar and unbalanced hole/electron mobility.

CONCLUSION

In summary, four electron-deficient compounds were synthesized and investigated as electron acceptor components in bulk heterojunction (BHJ) organic photovoltaic (OPV) cells. Detailed studies revealed that the αPPID and αPBDT exhibit improved the planarity in the perylene diimide (PDI) subunit, which strengthens close $\pi-\pi$ stacking. The absorption spectra αPPID and αPBDT show a strong tendency to form aggregates, because of the strong intermolecular $\pi-\pi$ interaction, which persists in blended films, leading to relatively high electron mobility. Inverted BHJ devices employing PTB7-Th as the donor and αPDI-based compounds as the acceptor demonstrate superior photovoltaic performance, relative to that using βPDI-based derivatives as the acceptor; an enhancement of 39% is obtained. The higher power conversion efficiency (PCE) of αPPID and αPBDT are mainly ascribed to their higher SCLC mobility and the more-efficient charge separation at interfaces with PTB7-Th. These results suggest that α-substituted PDI derivatives are indeed promising electron acceptors. Further exploration is underway to fulfill their potential in OPVs.

ASSOCIATED CONTENT

Supporting Information

The Supporting Information is available free of charge on the ACS Publications website at DOI: 10.1021/acs.chemmater.5b04570.

Experimental details, synthesis, theoretical calculation, UV-vis absorption spectra, photoluminescence spectra, 2D-GWIX, and device fabrication and characterization (PDF)

AUTHOR INFORMATION

Corresponding Author

*E-mail: lupingyu@uchicago.edu.

Author Contributions

$^{\nabla}$These authors made equal contributions to this work.

Funding

This work is supported by U.S. National Science Foundation grant (NSF Grant No. DMR-1263006) and NSF MRSEC program at the University of Chicago (No. DMR-0213745), DOE via the ANSER Center, an Energy Frontier Research Center funded by the U.S. Department of Energy, Office of Science, Office of Basic Energy Sciences, under Award No. DE-SC0001059 and NIST via CHIMAD program. W.C. gratefully acknowledges financial support from the U.S. Department of Energy, Office of Science, Office of Basic Energy Sciences, under Award No. KC020301.

Notes

The authors declare no competing financial interest.

ACKNOWLEDGMENTS

We thank James (Matt) Kurley and Dr. Jaeyong Jang (Talapin Group, University of Chicago) and Dr. Inhwan Jung (Korea Research Institute of Chemical Technology) for physical measurement discussion and help. We also thank Lan Luo and Dr. Chuan Wang (Yamamoto Group, University of Chicago) for synthetic discussion and share of equipment.

REFERENCES

(1) Lu, L.; Zheng, T.; Wu, Q.; Schneider, A. M.; Zhao, D.; Yu, L. Recent Advances in Bulk Heterojunction Polymer Solar Cells. *Chem. Rev.* **2015**, *115*, 12666.

(2) Chen, C. C.; Chang, W. H.; Yoshimura, K.; Ohya, K.; You, J.; Gao, J.; Hong, Z.; Yang, Y. An efficient triple-junction polymer solar cell having a power conversion efficiency exceeding 11%. *Adv. Mater.* **2014**, *26*, 5670−5677.

(3) Liang, Y.; Xu, Z.; Xia, J.; Tsai, S. T.; Wu, Y.; Li, G.; Ray, C.; Yu, L. For the bright future-bulk heterojunction polymer solar cells with power conversion efficiency of 7.4%. *Adv. Mater.* **2010**, *22*, E135−138.

(4) Kan, B.; Zhang, Q.; Li, M.; Wan, X.; Ni, W.; Long, G.; Wang, Y.; Yang, X.; Feng, H.; Chen, Y. Solution-processed organic solar cells based on dialkylthiol-substituted benzodithiophene unit with efficiency near 10%. *J. Am. Chem. Soc.* **2014**, *136*, 15529−15532.

(5) Subbiah, J.; Purushothaman, B.; Chen, M.; Qin, T.; Gao, M.; Vak, D.; Scholes, F. H.; Chen, X.; Watkins, S. E.; Wilson, G. J.; Holmes, A. B.; Wong, W. W.; Jones, D. J. Organic solar cells using a high-molecular-weight benzodithiophene−benzothiadiazole copolymer with an efficiency of 9.4%. *Adv. Mater.* **2015**, *27*, 702−705.

DOI: 10.1021/acs.chemmater.5b04570
Chem. Mater. 2016, 28, 1139−1146

(6) Liu, Y.; Zhao, J.; Li, Z.; Mu, C.; Ma, W.; Hu, H.; Jiang, K.; Lin, H.; Ade, H.; Yan, H. Aggregation and morphology control enables multiple cases of high-efficiency polymer solar cells. *Nat. Commun.* **2014**, *5*, 5293−5300.
(7) Eftaiha, F. A.; Sun, J.; Hill, I.; Welch, C. G. Recent advances of non-fullerene, small molecular acceptors for solution processed bulk heterojuction solar cells. *J. Mater. Chem. A* **2014**, *2*, 1201−1213.
(8) Li, W.; Roelofs, W. S.; Turbiez, M.; Wienk, M. M.; Janssen, R. A. Polymer solar cells with diketopyrrolopyrrole conjugated polymers as the electron donor and electron acceptor. *Adv. Mater.* **2014**, *26*, 3304−3309.
(9) Hwang, Y. J.; Courtright, B. A.; Ferreira, A. S.; Tolbert, S. H.; Jenekhe, S. A. 7.7% Efficient All-Polymer Solar Cells. *Adv. Mater.* **2015**, *27*, 4578.
(10) Mori, D.; Benten, H.; Okada, I.; Ohkita, H.; Ito, S. Low-Bandgap Donor/Acceptor Polymer Blend Solar Cells with Efficiency Exceeding 4%. *Adv. Energy. Mater.* **2014**, *4*, 1301006−1301011.
(11) Zhou, Y.; Kurosawa, T.; Ma, W.; Guo, Y.; Fang, L.; Vandewal, K.; Diao, Y.; Wang, C.; Yan, Q.; Reinspach, J.; Mei, J.; Appleton, A. L.; Koleilat, G. I.; Gao, Y.; Mannsfeld, S. C.; Salleo, A.; Ade, H.; Zhao, D.; Bao, Z. High performance all-polymer solar cell via polymer side-chain engineering. *Adv. Mater.* **2014**, *26*, 3767−3772.
(12) Li, H.; Earmme, T.; Ren, G.; Saeki, A.; Yoshikawa, S.; Murari, N. M.; Subramaniyan, S.; Crane, M. J.; Seki, S.; Jenekhe, S. A. Beyond fullerenes: Design of nonfullerene acceptors for efficient organic photovoltaics. *J. Am. Chem. Soc.* **2014**, *136*, 14589−14597.
(13) Lin, Y.; Zhang, Z.-G.; Bai, H.; Wang, J.; Yao, Y.; Li, Y.; Zhu, D.; Zhan, X. High-performance fullerene-free polymer solar cells with 6.31% efficiency. *Energy Environ. Sci.* **2015**, *8*, 610−616.
(14) Facchetti, A. Polymer donor−polymer acceptor (all-polymer) solar cells. *Mater. Today* **2013**, *16*, 123−132.
(15) Zhao, J.; Li, Y.; Lin, H.; Liu, Y.; Jiang, K.; Mu, C.; Ma, T.; Lin Lai, J. Y.; Hu, H.; Yu, D.; Yan, H. High-efficiency non-fullerene organic solar cells enabled by a difluorobenzothiadiazole-based donor polymer combined with a properly matched small molecule acceptor. *Energy Environ. Sci.* **2015**, *8*, 520−525.
(16) Zhong, Y.; Trinh, M. T.; Chen, R.; Purdum, G. E.; Khlyabich, P. P.; Sezen, M.; Oh, S.; Zhu, H.; Fowler, B.; Zhang, B.; Wang, W.; Nam, C. Y.; Sfeir, M. Y.; Black, C. T.; Steigerwald, M. L.; Loo, Y. L.; Ng, F.; Zhu, X. Y.; Nuckolls, C. Molecular helices as electron acceptors in high-performance bulk heterojunction solar cells. *Nat. Commun.* **2015**, *6*, 8242−8249.
(17) Zhang, X.; Zhan, C.; Yao, J. Non-Fullerene Organic Solar Cells with 6.1% Efficiency through Fine-Tuning Parameters of the Film-Forming Process. *Chem. Mater.* **2015**, *27*, 166−173.
(18) Singh, R.; Aluicio-Sarduy, E.; Kan, Z.; Ye, T.; MacKenzie, R. C. I.; Keivanidis, P. E. Fullerene-free organic solar cells with an efficiency of 3.7% based on a low-cost geometrically planar perylene diimide monomer. *J. Mater. Chem. A* **2014**, *2*, 14348−14353.
(19) Wurthner, F.; Saha-Möller, C. R.; Fimmel, B.; Ogi, S.; Leowanawat, P. Assemblies as Archetype Functional Supramolecular Materials. *Chem. Rev.* **2015**, 150813114318005.
(20) Liu, Y.; Lai, J. Y. L.; Chen, S.; Li, Y.; Jiang, K.; Zhao, J.; Li, Z.; Hu, H.; Ma, T.; Lin, H.; Liu, J.; Zhang, J.; Huang, F.; Yu, D.; Yan, H. Efficient non-fullerene polymer solar cells enabled by tetrahedron-shaped core based 3D-structure small-molecular electron acceptors. *J. Mater. Chem. A* **2015**, *3*, 13632−13636.
(21) Rajaram, S.; Shivanna, R.; Kandappa, S. K.; Narayan, K. S. Nonplanar Perylene Diimides as Potential Alternatives to Fullerenes in Organic Solar Cells. *J. Phys. Chem. Lett.* **2012**, *3*, 2405−2408.
(22) Jiang, W.; Ye, L.; Li, X.; Xiao, C.; Tan, F.; Zhao, W.; Hou, J.; Wang, Z. Bay-linked perylene bisimides as promising non-fullerene acceptors for organic solar cells. *Chem. Commun. (Cambridge, U. K.)* **2014**, *50*, 1024−1026.
(23) Shivanna, R.; Shoaee, S.; Dimitrov, S.; Kandappa, S. K.; Rajaram, S.; Durrant, J. R.; Narayan, K. S. Charge generation and transport in efficient organic bulk heterojunction solar cells with a perylene acceptor. *Energy Environ. Sci.* **2014**, *7*, 435−441.
(24) Zang, Y.; Li, C. Z.; Chueh, C. C.; Williams, S. T.; Jiang, W.; Wang, Z. H.; Yu, J. S.; Jen, A. K. Integrated molecular, interfacial, and device engineering towards high-performance non-fullerene based organic solar cells. *Adv. Mater.* **2014**, *26*, 5708−5714.
(25) Zhong, Y.; Trinh, M. T.; Chen, R.; Wang, W.; Khlyabich, P. P.; Kumar, B.; Xu, Q.; Nam, C. Y.; Sfeir, M. Y.; Black, C.; Steigerwald, M. L.; Loo, Y. L.; Xiao, S.; Ng, F.; Zhu, X. Y.; Nuckolls, C. Efficient organic solar cells with helical perylene diimide electron acceptors. *J. Am. Chem. Soc.* **2014**, *136*, 15215−15221.
(26) Sun, D.; Meng, D.; Cai, Y.; Fan, B.; Li, Y.; Jiang, W.; Huo, L.; Sun, Y.; Wang, Z. Non-Fullerene-Acceptor-Based Bulk-Heterojunction Organic Solar Cells with Efficiency over 7%. *J. Am. Chem. Soc.* **2015**, *137*, 11156−11162.
(27) Yan, Q.; Zhou, Y.; Zheng, Y.-Q.; Pei, J.; Zhao, D. Towards rational design of organic electron acceptors for photovoltaics: A study based on perylenediimide derivatives. *Chem. Sci.* **2013**, *4*, 4389−4394.
(28) Huang, C.; Barlow, S.; Marder, S. R. Perylene-3,4,9,10-tetracarboxylic acid diimides: synthesis, physical properties, and use in organic electronics. *J. Org. Chem.* **2011**, *76*, 2386−2407.
(29) Oh, J. H.; Liu, S.; Bao, Z.; Schmidt, R.; Würthner, F. Air-stable *n*-channel organic thin-film transistors with high field-effect mobility based on *N*,*N*′-bis(heptafluorobutyl)-3,4:9,10-perylene diimide. *Appl. Phys. Lett.* **2007**, *91*, 212107−212109.
(30) Schmidt, R.; Oh, J. H.; Sun, Y. S.; Deppisch, M.; Krause, A. M.; Radacki, K.; Braunschweig, H.; Konemann, M.; Erk, P.; Bao, Z.; Wurthner, F. High-performance air-stable *n*-channel organic thin film transistors based on halogenated perylene bisimide semiconductors. *J. Am. Chem. Soc.* **2009**, *131*, 6215−6228.
(31) Gsanger, M.; Oh, J. H.; Konemann, M.; Hoffken, H. W.; Krause, A. M.; Bao, Z.; Wurthner, F. A crystal-engineered hydrogen-bonded octachloroperylene diimide with a twisted core: An *n*-channel organic semiconductor. *Angew. Chem., Int. Ed.* **2010**, *49*, 740−743.
(32) Teraoka, T.; Hiroto, S.; Shinokubo, H. Iridium-catalyzed direct tetraborylation of perylene bisimides. *Org. Lett.* **2011**, *13*, 2532−2535.
(33) Nakazono, S.; Imazaki, Y.; Yoo, H.; Yang, J.; Sasamori, T.; Tokitoh, N.; Cedric, T.; Kageyama, H.; Kim, D.; Shinokubo, H.; Osuka, A. Regioselective Ru-catalyzed direct 2,5,8,11-alkylation of perylene bisimides. *Chem.—Eur. J.* **2009**, *15*, 7530−7533.
(34) Nakazono, S.; Easwaramoorthi, S.; Kim, D.; Shinokubo, H.; Osuka, A. Synthesis of arylated perylene bisimides through C-H bond cleavage under ruthenium catalysis. *Org. Lett.* **2009**, *11*, 5426−5429.
(35) Battagliarin, G.; Li, C.; Enkelmann, V.; Mullen, K. 2,5,8,11-Tetraboronic ester perylenediimides: A next generation building block for dye-stuff synthesis. *Org. Lett.* **2011**, *13*, 3012−3015.
(36) Hartnett, P. E.; Timalsina, A.; Matte, H. S. S. R.; Zhou, N.; Guo, X.; Zhao, W.; Facchetti, A.; Chang, R. P. H.; Hersam, M. C.; Wasielewski, M. R.; Marks, T. J. Slip-Stacked Perylenediimides as an Alternative Strategy for High Efficiency Nonfullerene Acceptors in Organic Photovoltaics. *J. Am. Chem. Soc.* **2014**, *136*, 16345−16356.
(37) Teraoka, T.; Hiroto, S.; Shinokubo, H. Iridium-Catalyzed Direct Tetraborylation of Perylene Bisimides. *Org. Lett.* **2011**, *13*, 2532−2535.
(38) Ahmed, E.; Ren, G.; Kim, F. S.; Hollenbeck, E. C.; Jenekhe, S. A. Design of New Electron Acceptor Materials for Organic Photovoltaics: Synthesis, Electron Transport, Photophysics, and Photovoltaic Properties of Oligothiophene-Functionalized Naphthalene Diimides. *Chem. Mater.* **2011**, *23*, 4563−4577.
(39) Zhang, X.; Lu, Z.; Ye, L.; Zhan, C.; Hou, J.; Zhang, S.; Jiang, B.; Zhao, Y.; Huang, J.; Zhang, S.; Liu, Y.; Shi, Q.; Liu, Y.; Yao, J. A Potential Perylene Diimide Dimer-Based Acceptor Material for Highly Efficient Solution-Processed Non-Fullerene Organic Solar Cells with 4.03% Efficiency. *Adv. Mater.* **2013**, *25*, 5791−5797.
(40) Jung, I. H.; Lo, W.-Y.; Jang, J.; Chen, W.; Zhao, D.; Landry, E. S.; Lu, L.; Talapin, D. V.; Yu, L. Synthesis and Search for Design Principles of New Electron Accepting Polymers for All-Polymer Solar Cells. *Chem. Mater.* **2014**, *26*, 3450−3459.
(41) Zou, L.; Wang, X. Y.; Zhang, X. X.; Dai, Y. Z.; Wu, Y. D.; Wang, J. Y.; Pei, J. Toward electron-deficient pyrene derivatives: Construction

DOI: 10.1021/acs.chemmater.5b04570
Chem. Mater. 2016, 28, 1139−1146

of pyrene tetracarboxylic diimide containing five-membered imide rings. *Chem. Commun. (Cambridge, U. K.)* **2015**, *51*, 12585−12588.
(42) Crawford, A. G.; Liu, Z.; Mkhalid, I. A.; Thibault, M. H.; Schwarz, N.; Alcaraz, G.; Steffen, A.; Collings, J. C.; Batsanov, A. S.; Howard, J. A.; Marder, T. B. Synthesis of 2- and 2,7-functionalized pyrene derivatives: An application of selective C−H borylation. *Chem.—Eur. J.* **2012**, *18*, 5022−5035.
(43) Singh, T. B.; Erten, S.; Günes, S.; Zafer, C.; Turkmen, G.; Kuban, B.; Teoman, Y.; Sariciftci, N. S.; Icli, S. Soluble derivatives of perylene and naphthalene diimide for *n*-channel organic field-effect transistors. *Org. Electron.* **2006**, *7*, 480−489.
(44) Zhao, Z.; Zhang, F.; Zhang, X.; Yang, X.; Li, H.; Gao, X.; Di, C.-a.; Zhu, D. 1,2,5,6-Naphthalenediimide Based Donor−Acceptor Copolymers Designed from Isomer Chemistry for Organic Semiconducting Materials. *Macromolecules* **2013**, *46*, 7705−7714.
(45) Dennler, G.; Scharber, M. C.; Brabec, C. J. Polymer−Fullerene Bulk-Heterojunction Solar Cells. *Adv. Mater.* **2009**, *21*, 1323−1338.
(46) Ford, W. E.; Kamat, P. V. Photochemistry of 3,4,9,10-perylenetetracarboxylic dianhydride dyes. 3. Singlet and triplet excited-state properties of the bis(2,5-di-*tert*-butylphenyl)imide derivative. *J. Phys. Chem.* **1987**, *91*, 6373−6380.
(47) Gómez, R.; Veldman, D.; Blanco, R.; Seoane, C.; Segura, J. L.; Janssen, R. A. J. Energy and Electron Transfer in a Poly(fluorene-alt-phenylene) Bearing Perylenediimides as Pendant Electron Acceptor Groups. *Macromolecules* **2007**, *40*, 2760−2772.
(48) Ramanan, C.; Kim, C. H.; Marks, T. J.; Wasielewski, M. R. Excitation Energy Transfer within Covalent Tetrahedral Perylenediimide Tetramers and Their Intermolecular Aggregates. *J. Phys. Chem. C* **2014**, *118*, 16941−16950.
(49) Zhou, Y.; Ding, L.; Shi, K.; Dai, Y. Z.; Ai, N.; Wang, J.; Pei, J. A non-fullerene small molecule as efficient electron acceptor in organic bulk heterojunction solar cells. *Adv. Mater.* **2012**, *24*, 957−961.
(50) Chen, Z.; Stepanenko, V.; Dehm, V.; Prins, P.; Siebbeles, L. D.; Seibt, J.; Marquetand, P.; Engel, V.; Wurthner, F. Photoluminescence and conductivity of self-assembled $\pi-\pi$ stacks of perylene bisimide dyes. *Chem.—Eur. J.* **2007**, *13*, 436−449.
(51) Giaimo, J. M.; Lockard, J. V.; Sinks, L. E.; Scott, A. M.; Wilson, T. M.; Wasielewski, M. R. Excited singlet states of covalently bound, cofacial dimers and trimers of perylene-3,4:9,10-bis(dicarboximide)s. *J. Phys. Chem. A* **2008**, *112*, 2322−2330.
(52) Frisch, M. J.; Trucks, G. W.; Schlegel, H. B.; Scuseria, G. E.; Robb, M. A.; Cheeseman, J. R.; Scalmani, G.; Barone, V.; Mennucci, B.; Petersson, G. A.; Nakatsuji, H.; Caricato, M.; Li, X.; Hratchian, H. P.; Izmaylov, A. F.; Bloino, J.; Zheng, G.; Sonnenberg, J. L.; Hada, M.; Ehara, M.; Toyota, K.; Fukuda, R.; Hasegawa, J.; Ishida, M.; Nakajima, T.; Honda, Y.; Kitao, O.; Nakai, H.; Vreven, T.; Montgomery, J. A., Jr.; Peralta, J. E.; Ogliaro, F.; Bearpark, M.; Heyd, J. J.; Brothers, E.; Kudin, K. N.; Staroverov, V. N.; Kobayashi, R.; Normand, J.; Raghavachari, K.; Rendell, A.; Burant, J. C.; Iyengar, S. S.; Tomasi, J.; Cossi, M.; Rega, N.; Millam, J. M.; Klene, M.; Knox, J. E.; Cross, J. B.; Bakken, V.; Adamo, C.; Jaramillo, J.; Gomperts, R.; Stratmann, R. E.; Yazyev, O.; Austin, A. J.; Cammi, R.; Pomelli, C.; Ochterski, J. W.; Martin, R. L.; Morokuma, K.; Zakrzewski, V. G.; Voth, G. A.; Salvador, P.; Dannenberg, J. J.; Dapprich, S.; Daniels, A. D.; Farkas, O.; Foresman, J. B.; Ortiz, J. V.; Cioslowski, J.; Fox, D. J. *Gaussian 09, Revision D.01*; Gaussian, Inc.: Wallingford, CT, 2013.
(53) Marsh, R. A.; Groves, C.; Greenham, N. C. A microscopic model for the behavior of nanostructured organic photovoltaic devices. *J. Appl. Phys.* **2007**, *101*, 083509−083515.
(54) Guo, X.; Zhou, N.; Lou, S. J.; Smith, J.; Tice, D. B.; Hennek, J. W.; Ortiz, R. P.; Navarrete, J. T. L.; Li, S.; Strzalka, J.; Chen, L. X.; Chang, R. P. H.; Facchetti, A.; Marks, T. J. Polymer solar cells with enhanced fill factor. *Nat. Photonics* **2013**, *7*, 825−833.
(55) Lu, R.-Q.; Zheng, Y.-Q.; Zhou, Y.-N.; Yan, X.-Y.; Lei, T.; Shi, K.; Zhou, Y.; Pei, J.; Zoppi, L.; Baldridge, K. K.; Siegel, J. S.; Cao, X.-Y. Corannulene derivatives as non-fullerene acceptors in solution-processed bulk heterojunction solar cells. *J. Mater. Chem. A* **2014**, *2*, 20515−20519.
(56) Li, Z.; Lin, J. D. A.; Phan, H.; Sharenko, A.; Proctor, C. M.; Zalar, P.; Chen, Z.; Facchetti, A.; Nguyen, T.-Q. Competitive Absorption and Inefficient Exciton Harvesting: Lessons Learned from Bulk Heterojunction Organic Photovoltaics Utilizing the Polymer Acceptor P(NDI2OD-T2). *Adv. Funct. Mater.* **2014**, *24*, 6989−6998.
(57) Lu, L.; Xu, T.; Chen, W.; Landry, E. S.; Yu, L. Ternary blend polymer solar cells with enhanced power conversion efficience. *Nat. Photonics* **2014**, *8*, 716−722.
(58) Koster, L. J. A.; Mihailetchi, V. D.; Xie, H.; Blom, P. W. M. Origin of the light intensity dependence of the short-circuit current of polymer/fullerene solar cells. *Appl. Phys. Lett.* **2005**, *87*, 203502−203504.

DOI: 10.1021/acs.chemmater.5b04570
Chem. Mater. 2016, 28, 1139−1146